Photoluminescence properties and energy level of RE (RE = Pr, Sm, Tb, Er, Dy) in $Y_4Si_2O_7N_2$

Wang, Guo-Jun; Pan, Dong-Jie; Xu, Tao; Xiang, Guang-Xin; Zhang, Zhi-Jun; Hintzen, Hubertus T.; Zhao, Jing-Tai; Huang, Yan

DOI
10.1016/j.jallcom.2017.02.298

Publication date
2017

Document Version
Final published version

Published in
Journal of Alloys and Compounds

Journal of Alloys and Compounds 708 (2017) 154–161

Contents lists available at ScienceDirect

Journal of Alloys and Compounds

journal homepage: http://www.elsevier.com/locate/jalcom

Photoluminescence properties and energy level of *RE* (*RE* = Pr, Sm, Tb, Er, Dy) in $Y_4Si_2O_7N_2$

Guo-Jun Wang [a], Dong-Jie Pan [a], Tao Xu [a], Guang-Xin Xiang [a], Zhi-Jun Zhang [a, *], Hubertus T. Hintzen [b], Jing-Tai Zhao [a], Yan Huang [c]

[a] School of Materials Science and Engineering, Shanghai University, Shanghai 200072, PR China
[b] Luminescent Materials Research Group, Delft University of Technology, Mekelweg 15, 2629 JB Delft, The Netherlands
[c] Institute of High Energy Physics, Chinese Academy of Science, Beijing 100039, PR China

ARTICLE INFO

Article history:
Received 21 September 2016
Received in revised form
26 February 2017
Accepted 27 February 2017
Available online 1 March 2017

Keywords:
Photoluminescence
$Y_4Si_2O_7N_2$
Energy level
RE^{3+}-activated
Silicon-oxynitride

ABSTRACT

RE^{3+} (*RE* = Pr, Sm, Tb, Er, Dy)-activated $Y_4Si_2O_7N_2$ samples were prepared by a solid-state reaction method at high temperature, and their photoluminescence properties were investigated. The absorption band located at about 250 nm is attributed to the host absorption. The 5*d* bands of Pr^{3+} and Tb^{3+} are at rather low energy in $Y_4Si_2O_7N_2$ compared to oxide. The direct Pr^{3+} $4f^2 \rightarrow 4f^15d^1$ excitation at 275 nm leads to typical $4f^2 \rightarrow 4f^2$ line emissions (450–700 nm) and strong $4f^15d^1 \rightarrow 4f^2$ broad band emission (300–450 nm), respectively. The charge transfer ($N^{3-} \rightarrow Sm^{3+}$) band of Sm^{3+} was observed at a somewhat lower energy of 4.68 eV compared to oxide, and Sm^{3+}-activated sample shows a bright red emission originating from $^4G_{5/2} \rightarrow {}^6H_J$ (J = 5/2, 7/2 and 9/2) transitions. For Tb^{3+}-doped sample, the direct Tb^{3+} $4f^8 \rightarrow 4f^75d^1$ excitation leads to $^5D_3 \rightarrow {}^7F_J$ (J = 6, 5, 4, 3) (blue) and $^5D_4 \rightarrow {}^7F_J$ (J = 6, 5, 4, 3) (green) line emissions, the cross-relaxation depended on Tb concentration has happened. The incorporation of Er^{3+} (or Dy^{3+}) into $Y_4Si_2O_7N_2$ resulted in a typical Er^{3+} (or Dy^{3+}) *f-f* line absorptions and emissions. Moreover, the energy transfer from the host lattice to the luminescent activators (Pr^{3+}, Tb^{3+} and Sm^{3+}) is observed. The energy level diagram containing the position of 4*f* and 5*d* energy levels of all Ln^{2+} and Ln^{3+} ions relative to the valence and conduction band of $Y_4Si_2O_7N_2$ has been established and studied based on the data presented in this work, and further provides a platform for studying the photoluminescence properties as well as the valence stability of the lanthanide ions.

1. Introduction

In recent years, research on silicon-nitride and silicon-oxynitride based materials for solid state lighting have attracted increasing attentions in the academic and industrial fields [1–4]. Compared with conventional incandescent and fluorescent lamps, there are many advantages for the phosphor-converted white-light emitting diodes (WLEDs) in the real world, such as the higher efficiency, lower power consumption, longer lifetime and being more environmental-friendly [5–7]. For nitride or oxynitride-based hosts used for WLED, nitride or oxynitride-based hosts are new blue excitable red-emitting phosphors, compared to the yellow-emitting Ce^{3+}-doped garnet phosphor (i.e. YAG:Ce^{3+}) with the disadvantages of being low color-rendering index (CRI) and high color temperature due to lack of red emission [8]. On the other hand, the several competitive advantages including high chemical stability, excellent thermal quenching property make it possible that the nitride/oxynitride-based hosts are good candidates for near ultraviolet (*n*-UV) WLED to carve out a dominant position in WLED market in the near future, compared to oxide, sulfide and halide-based phosphors [9,10].

In the *Ln*-Si-O-N quaternary system, the rare-earth silicon-oxynitrides of $Ln_4Si_2O_7N_2$ (*Ln* = Y, Lu, Gd and La) have been prepared and their photoluminescence properties (Ce^{3+}/Tb^{3+}-activated) were investigated [11–15]. Y_2O_3 as one of starting materials also plays a role of the sintering additives during the preparation of the $Y_4Si_2O_7N_2$. The quaternary crystals would occurred in the sintering process, mostly as grain boundary phases [11,16]. The $Y_4Si_2O_7N_2$ structure typically consists of $Si[O/N]_4$ tetrahedra, similar to the silicates, giving rise to the advantages of the excellent thermal and chemical stability (Fig. S1 in supporting information).

* Corresponding author.
E-mail address: zhangzhijun@shu.edu.cn (Z.-J. Zhang).

http://dx.doi.org/10.1016/j.jallcom.2017.02.298
0925-8388/

$Si[O/N]_4$ units are stacked together by sharing their corners or edges to form a relatively condensed $Si[O/N]_4$ framework [17]. So, the $Y_4Si_2O_7N_2$ is a good potential silicon-oxynitrides host for *n*-UV-emitting phosphor. However, critical synthesis conditions, such as high temperature and high pressure, are required for the synthesis of most nitride/oxynitride materials. J.W.H. van Krevel et al. [14] have reported the long wavelength emission of Ce^{3+} in $Y_4Si_2O_7N_2$. Sun et al. have reported the low theoretical minimum thermal conductivity of $Y_4Si_2O_7N_2$ by first-principles calculation and verified by experiment [18]. And Y.H. Wang et al. have reported the crystal structure of Ce-doped $Y_4Si_2O_7N_2$ and luminescence properties, which exhibited emission colors that can be tuned from blue to green [19]. In addition, the energy transfer in Ce^{3+}/Tb^{3+}-activated $Y_4Si_2O_7N_2$ phosphors was also investigated by Z.G. Xia et al. [20] Until now, there is no investigation on the luminescence properties of other rare-earth ions in $Y_4Si_2O_7N_2$ except Ce^{3+} and Tb^{3+}. Herein, we focus on investigating the photoluminescence properties of rare-earth ions (*RE* = Pr, Sm, Tb, Er and Dy) in $Y_4Si_2O_7N_2$, moreover, the energy level scheme for $Y_4Si_2O_7N_2$ is constructed and used as a tool to study the luminescence mechanism of these rare-earth ions in $Y_4Si_2O_7N_2$.

2. Materials and methods

2.1. Experimental section

$Y_{3.88}RE_{0.12}Si_2O_7N_2$ (*RE* = Pr, Sm, Tb, Er, Dy) samples were prepared by solid-state reaction at high temperature. The starting materials were analytical grade SiO_2, Si_3N_4, and rare-earth oxides (Y_2O_3, Pr_6O_{11}, Sm_2O_3, Tb_4O_7, Er_2O_3, Dy_2O_3, 99.99% purity). The nominal doped lanthanide concentrations were 3 mol% relative to yttrium. Appropriate amount of starting materials were weighed, thoroughly mixed, and ground in an agate mortar. The powder mixtures were sintered in molybdenum crucibles at 1650 °C for 4 h in a horizontal tube furnace under reducing atmosphere (N_2/H_2 = 95:5). After sintering, these samples were gradually furnace-cooled to room temperature and ground into power for further analysis. And the prepared samples had no apparent reaction with the molybdenum crucibles.

2.2. Sample characterization and calculation

To speculate the site occupancy of RE^{3+} in $Y_4Si_2O_7N_2$, total energy calculations of un-doped and Tb^{3+}-doped $Y_4Si_2O_7N_2$ (2 × 1 × 1 supercell) crystals were carried out by the planewave-seudo potential CASTEP code. Perdew-Burke-Ernzerhof (PBE) functional in general gradient approximation (GGA) was adopted as the framework to solve Kohn-Sham equation iteratively based on density mixing technique, while ultra-soft format of potentials suggested by Vanderbilt were selected from a database provided along with CASTEP. The plane wave cut-off energy was chosen at 450 eV and kept unchanged throughout. The Broyden-Fletcher-Goldfarb-Shanno (BFGS) method was used to relax the crystal structure to its ground state. In this stage, a Monkhorst-Pack *k* point mesh of 4 × 4 × 2 was used, and the convergence threshold were 1.0×10^{-6} eV/atom for total energy, 0.03 eV/Å for forces, 0.03 GPa for stress, and 5×10^{-4} Å for ionic displacement, respectively.

It is of note that there are four different sites for Y^{3+} ions, namely Y(1), Y(2), Y(3) and Y(4) in $Y_4Si_2O_7N_2$. In the four distinguishable Y sites, three Y ions are seven-coordinated with O and N atoms (usually be defined as Y(1), Y(2) and Y(4)), and the fourth Y ion (usually be defined as Y(3)) is in a six-fold coordination. In addition, every Y site in $Y_4Si_2O_7N_2$ exhibits the Wyckoff symbol 4e (site symmetry *C*1). What's more, the Y(1) and Y(2) sites are coordinated with three oxygen ions, and Y(3) and Y(4) sites are surrounded by one oxygen ion, as shown in Table 1.

As is well known, the exact ordering of O/N anions around the cation sites in the unit cell determines the result of calculation [21]. For a detailed calculation and interpretation of the total energies of $Y_4Si_2O_7N_2$ doped with the Tb^{3+} ions locating at four different Y sites, the suggested crystal structure of $Y_4Si_2O_7N_2$ was derived from *J*-phase of $Y_4Si_2O_7N_2$ [17]. The positions of Y and Si are well determined. However, the O/N distribution has been a subject of discussion [11,19,22]. Thus, the model concerning the fixed occupation of the O/N anions has been established based on the crystallographic data reported in the literature [17] (Table 1), including relaxation of the unit cell shape and dimensions and then calculate the total energy. Herein, Tb concentration was set to 10 mol% at four different Y sites, the potentials will be $V = 0.1\ V_{Tb}(k) + 0.9\ V_Y(k)$. Total energy of doped crystals was compared and possible preferred site occupancy of Tb dopants was pointed out accordingly.

The X-ray diffraction (XRD) patterns were collected in a 2θ range of 10–75° using D/max-2550 X-ray diffraction meter (18 kV, 10 mA). The step scan with a step size of 0.02° and a count time of 1 s per step were used for collecting all XRD patterns. The XRD measurements were performed at room temperature in air. Diffuse

Table 1
The atomic position of Y(1), Y(2), Y(3), Y(4) in the unit cell (the first row), occupation of the O/N anions around Y atoms (the second row), the Y–O/N bond length (the third row), along with the binding energy of $Y_4Si_2O_7N_2$: Tb^{3+} (10 mol%) with different Y^{3+} crystallographic sites occupied by Tb^{3+} (the lasted row). All values for the bond length and energy are in Å and eV, respectively. The occupancy of O/N anions is fixed at 0.8333/0.1667 for all the O/N sites [17].

Un-doped	Tb@Y(1)	Tb@Y(2)	Tb@Y(3)	Tb@Y(4)
	(0.16718, 0.62140, 0.07100)	(0.33582, 0.12268, 0.41730)	(0.47192, 0.91351, 0.18930)	(0.02319, 0.40240, 0.28820)
	(0.16718, 0.87860, 0.57100)	(0.66418, 0.62268, 0.08270)	(0.47192, 0.58649, 0.68930)	(0.97681, 0.90240, 0.21150)
	(0.83282, 0.37860, 0.92900)	(0.66418, 0.87732, 0.58270)	(0.52808, 0.08649, 0.81070)	(0.97681, 0.59760, 0.71150)
	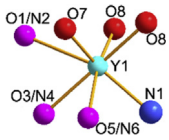	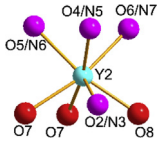	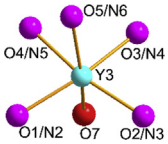	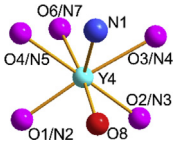
	Y1–N1: 2.329	Y2–O2/N3: 2.696	Y3–O1/N2: 2.312	Y4–N1: 2.484
	Y1–O1/N2: 2.771	Y2–O4/N5: 2.309	Y3–O2/N3: 2.273	Y4–O1/N2: 2.318
	Y1–O3/N4: 2.422	Y2–O5/N6: 2.285	Y3–O3/N4: 2.264	Y4–O2/N3: 2.387
	Y1–O5/N6: 2.696	Y2–O6/N7: 2.303	Y3–O4/N5: 2.338	Y4–O3/N4: 2.592
	Y1–O7: 2.317	Y2–O7: 2.301	Y3–O5/N6: 2.365	Y4–O4/N5: 2.599
	Y1–O8: 2.244	Y2–O7: 2.272	Y3–O7: 2.225	Y4–O6/N7: 2.301
	Y1–O8: 2.265	Y2–O8: 2.163		Y4–O8: 2.289
−18375.62	−18886.28	−18882.63	−18880.13	−18885.97

reflectance spectrum in the UV and visible range was measured with a Cary 5000 spectrophotometer (Varian Inc., USA) with a Xe flash lamp, and the data was calibrated with the reflection of barium sulphate ($BaSO_4$, reflection ~ 100%). UV excitation and emission spectra, were measured at Hitachi F-4600 spectrometer. The scan speed was fixed at 240 nm/min, the voltage was 400 V and the slits were fixed at 2.5 nm. All of the luminescence spectra were recorded at room temperature.

3. Results and discussion

3.1. Phase formation of $Y_{3.88}RE_{0.12}Si_2O_7N_2$ (RE = Pr, Sm, Tb, Er, Dy)

Fig. 1 shows the powder XRD patterns of *RE* (*RE* = Pr, Sm, Tb, Er, Dy)-doped $Y_4Si_2O_7N_2$ samples, along with standard $Y_4Si_2O_7N_2$ (JCPDS card No. 86–1106). By taking into account the sizes of cations and their coordination, it is assumed that the RE^{3+} substitution would occur at four possible Y^{3+} sites, due to the fact that the ionic radii of Pr^{3+} ($r = 0.99$ Å, CN = 6), Sm^{3+} ($r = 0.958$ Å, CN = 6), Tb^{3+} ($r = 0.923$ Å, CN = 6), Er^{3+} ($r = 0.89$ Å, CN = 6) and Dy^{3+} ($r = 0.912$ Å, CN = 6) are similar to that of Y^{3+} ($r = 0.90$ Å, CN = 6) [23].

By calculation, total binding energies of un-doped and Tb^{3+}-doped $Y_4Si_2O_7N_2$ were tabulated in Table 1. All values are in eV per unit cell. From the calculation in Table 1, when the Y(1) site was occupied by Tb, the doped system possesses the lowest total binding energy, indicating that the Y(1) site is the most stable site for Tb to occupy compared with Y(2), Y(3) and Y(4) sites.

3.2. Diffuse reflection spectrum and optical band gap of un-doped $Y_4Si_2O_7N_2$

Fig. 2a illustrates the diffuse reflection spectrum of un-doped $Y_4Si_2O_7N_2$, which exhibits a strong drop in the reflection in the UV range below 280 nm, corresponding to the band transition in the $Y_4Si_2O_7N_2$ host lattice. In addition, the absorption spectrum of $Y_4Si_2O_7N_2$ was calculated from the reflection spectrum by using the Kubelka-Munk function (Eq. (1)) to better localize the threshold for the host lattice absorption,

$$F(R) = (1 - R)^2 \big/ 2R = K/S \quad (1)$$

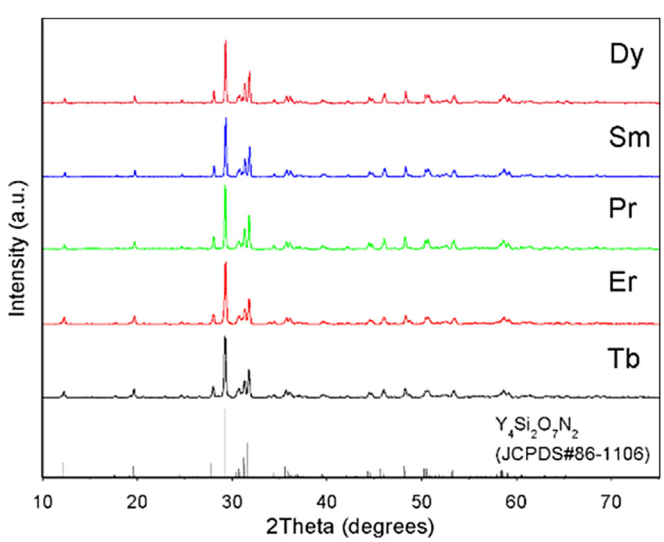

Fig. 1. X-ray power diffraction patterns of standard $Y_4Si_2O_7N_2$, $Y_{3.88}Tb_{0.12}Si_2O_7N_2$, $Y_{3.88}Er_{0.12}Si_2O_7N_2$, $Y_{3.88}Pr_{0.12}Si_2O_7N_2$, $Y_{3.88}Sm_{0.12}Si_2O_7N_2$, $Y_{3.88}Dy_{0.12}Si_2O_7N_2$.

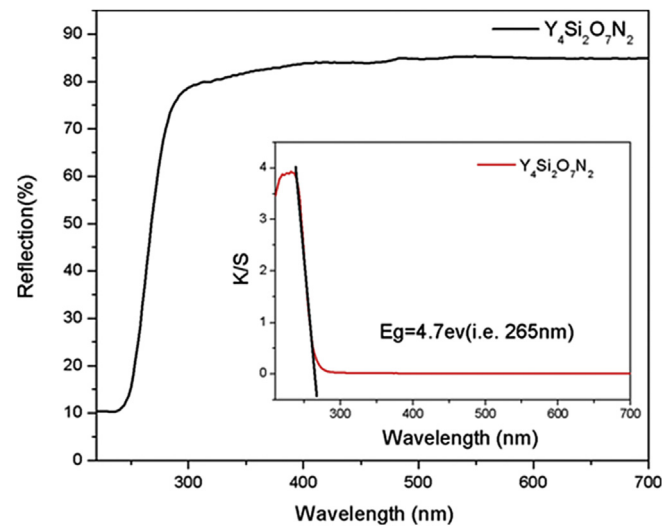

Fig. 2. Diffuse reflection spectrum (a) and absorption spectrum calculated by the Kubelka-Munk formula (b) of $Y_4Si_2O_7N_2$.

In which, *R* refers to the reflection, *K* represents the absorption coefficient and *S* is the scattering coefficient, respectively. The absorption (*K*/*S*) function of $Y_4Si_2O_7N_2$ derived with the Kubelka-Munk equation is shown in Fig. 2b. The value of the optical band gap of $Y_4Si_2O_7N_2$ is calculated by virtue of extrapolating the Kubelka-Munk equation to $K/S = 0$. There is one absorption band located at 235 nm, and the optical band gap of the $Y_4Si_2O_7N_2$ is evaluated to be 4.7 eV (i.e. 265 nm).

3.3. Photoluminescence of $Y_{3.88}Pr_{0.12}Si_2O_7N_2$

It is well known that the energy level structure of the Pr^{3+} ion with two 4*f* electrons ($4f^2$) contains several 4*f*-4*f* transitions. The diffuse reflection spectrum of $Y_{3.88}Pr_{0.12}Si_2O_7N_2$ shows a broad absorption edge located at about 275 nm (Fig. 3 (a)). Besides, a group of weak absorption lines at long-wavelength can be observed in the wavelength range of 425–500 nm, which are ascribed to $^3H_4 \rightarrow {}^3P_2$ (~444 nm), $^3H_4 \rightarrow {}^3P_1$ (~472 nm) and $^3H_4 \rightarrow {}^3P_0$ (~486 nm) transitions of Pr^{3+} ions, respectively. Excitation spectra by monitoring the $4f^2 \rightarrow 4f^2$ emissions are also presented in Fig. 3(a). Consistent with the diffuse reflectance spectrum, several weak $4f^2 \rightarrow 4f^2$ transitions of Pr^{3+} can be observed in the wavelength range of 425–500 nm in the excitation spectra. Besides, an excitation band with the peak located at about 275 nm in the wavelength range from 240 to 310 nm is observed, which is related to the $4f^2 \rightarrow 4f^15d^1$ transition of Pr^{3+} other than the host absorption. The optical band gap of the host lattice is around 4.68 eV (or 265 nm), so the host absorption may be located at higher energy region, and it may be entirely overlapped in the band with peak at 275 nm, which will further be discussed below.

Due to the direct $4f^2 \rightarrow 4f^15d^1$ excitation of Pr^{3+} around 275 nm, typical $4f^1 \rightarrow 5d^14f^2$ and $4f^2 \rightarrow 4f^2$ emissions of Pr^{3+} in the wavelength range of 300–700 nm were observed (Fig. 3 (b)). A board emission band (300–450 nm) occupies the higher energy district of the emission spectrum, which can be attributed to the $4f^15d^1 \rightarrow 4f^2$ ($^3H_4$, $^3H_5$) transitions. Besides, typical $4f^2 \rightarrow 4f^2$ emission lines (450–700 nm) of Pr^{3+} are observed in the emission spectra, which are assigned to transitions from $^3P_0 \rightarrow {}^3H_4$ (~503 nm), $^3P_0 \rightarrow {}^3H_5$ (~555 nm), $^3P_0 \rightarrow {}^3H_6$ (~630 nm) and $^3P_0 \rightarrow {}^3F_2$ (~667 nm) of Pr^{3+} ions, respectively. Moreover, the emission $^3P_0 \rightarrow {}^3H_4$ exhibits the strongest intensity. Due to the fact that the position of $4f^2$ [$^1S_0$] excited level (46800 cm^{-1}) is higher than the lowest $4f^15d^1$ state

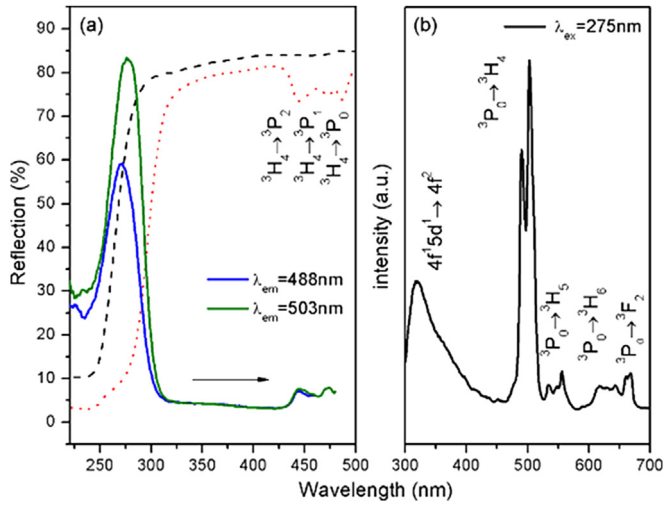

Fig. 3. (a) Diffuse reflection spectrum of $Y_{3.88}Pr_{0.12}Si_2O_7N_2$ (dotted line) compared with un-doped $Y_4Si_2O_7N_2$ (dashed line), and excitation spectra of $Y_{3.88}Pr_{0.12}Si_2O_7N_2$. (b) The emission spectra of $Y_{3.88}Pr_{0.12}Si_2O_7N_2$.

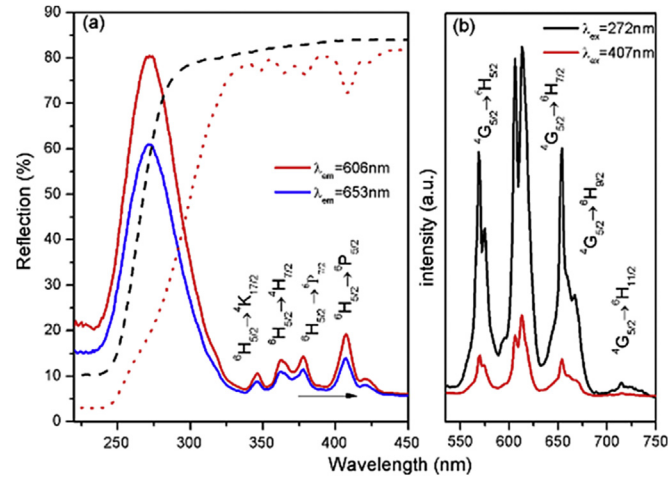

Fig. 4. (a) Diffuse reflection spectrum of Sm^{3+}-doped $Y_4Si_2O_7N_2$ (dotted line) compared with un-doped $Y_4Si_2O_7N_2$ (dashed line), and excitation spectra of $Y_{3.88}Sm_{0.12}Si_2O_7N_2$. (b) Typical emission spectra of $Y_{3.88}Sm_{0.12}Si_2O_7N_2$.

(36365 cm^{-1}) of Pr^{3+}, leading to the absence of the photo cascade emission ($^1S_0 \rightarrow {}^3P_1$, $^1I_6$ transitions) [24].

It is well known that the 5*d* levels of Ln^{3+} ions are at somewhat lower energy than the 5*d* orbital energy of the free RE^{3+} ions when they enter into host lattice. The 4*f*-5*d* transition energies of triply ionized lanthanides in various host compounds were provided by Dorenbos [25,26], and it was further proposed that the crystal field and covalency decrease $D(Ln, A)$ for the energy of the $4f^{n-1}5d$ levels of a lanthanide ion in certain compound *A* relative to the energies in the free ion, i.e.

$$D(Ln,\ A) = E(Ln,\ free) - E(Ln,\ A) \tag{2}$$

is almost independent of the nature of the lanthanide ion activated. In which, $E(Ln, \text{free})$ refers to the energy of the first *f*-*d* transition of Ln^{3+} as the free (gaseous) ion. $E(Ln, A)$ represents the energy of first *f*-*d* transition of the Ln^{3+}-doped in a certain compound *A* [27]. The lowest 4*f*-5*d* excitation transition of Ce^{3+}, $E(Ce^{3+}, Y_4Si_2O_7N_2)$ was measured at 395 nm (i.e. 25315 cm^{-1}). The 5*d* level of the free Ce^{3+} ion is 49340 cm^{-1} [25], thus, the *f*-*d* transition energy of Ce^{3+} in $Y_4Si_2O_7N_2$ is decreased by 24025 cm^{-1}, implying that $D(Ce^{3+}, Y_4Si_2O_7N_2)$ is about 24025 cm^{-1}. Ulteriorly, the $D\ (Ce^{3+}, Y_4Si_2O_7N_2)$ for energy of the $4f^{n-1}5d$ levels of Ce^{3+} in $Y_4Si_2O_7N_2$ can be used to predict the 5*d* energies of other lanthanides in this host lattice, due to the fact that the influence of the crystal field and covalency of the host lattice on the red shift of the 5*d* level is approximately equal for all *RE* ions. The 4*f*-5*d* transition of the free Pr^{3+} ion is reported to be 61580 cm^{-1} [25]. Therefore, the lowest *f*-*d* transition energy $E(Pr^{3+}, Y_4Si_2O_7N_2)$ of Pr^{3+} in $Y_4Si_2O_7N_2$ is calculated at 37555 cm^{-1} (263 nm) according to Eq. (2), in accordance with experimental results (275 nm, or 36365 cm^{-1}).

3.4. Photoluminescence of $Y_{3.88}Sm_{0.12}Si_2O_7N_2$

It is well known that divalent Sm^{2+} has the $4f^6$ electron configuration, similar to Eu^{3+} ([Xe] $4f^6$), thus Sm^{2+} can be excited into $4f^5 5d^1$ levels under irradiation with UV and visible light. However, there is a more complicated energy level structure and various possible transitions between *f* levels in Sm^{3+} ions, which exhibit a $4f^5$ configuration, so there are sharp line emissions.

Fig. 4(a) shows the diffuse reflection spectra and excitation spectra of $Y_{3.88}Sm_{0.12}Si_2O_7N_2$. The optical absorption edge at the short wavelength in the wavelength range of 230–290 nm in the reflection spectrum cannot be simply assigned to the absorption of the host lattice, due to the fact that the edge of the diffuse reflection of Sm^{3+}-doped sample is shifted to higher wavelength in comparison with un-doped sample. Typical sharp lines in the wavelength range of 340–450 nm ascribed to the transitions of $^6H_{5/2} \rightarrow {}^4H_{9/2}$ (~346 nm), $^6H_{5/2} \rightarrow {}^4D_{5/2}$ (~364 nm), $^6H_{5/2} \rightarrow {}^6P_{7/2}$ (~378 nm), $^6H_{5/2} \rightarrow {}^4F_{7/2}$ (~408 nm), $^6H_{5/2} \rightarrow {}^6P_{5/2}$ (~422 nm) [28] were recorded, consistent with the excitation spectrum. Beside the 4*f*-4*f* lines, there is a strong broad excitation band around 272 nm (FWHM ~ 0.8 eV) in the excitation spectra. This band cannot be attributed to 4*f*-5*d* transition of Sm^{3+}, on account of that the 4*f*-5*d* transition energy is estimated to be about 51815 cm^{-1} (193 nm) using the $D(Y_4Si_2O_7N_2)$ value of 24025 cm^{-1} and the free Sm^{3+} ion 4*f*-5*d* energy of 75840 cm^{-1} by virtue of Eq. (2) [25]. Generally, the value of energy of $O^{2-} \rightarrow Sm^{3+}$ charge transfer is usually larger than 5 eV, and it is well known that the energy of $N^{3-} \rightarrow Sm^{3+}$ charge transfer band is lower than that of $O^{2-} \rightarrow Sm^{3+}$ charge transfer band because of the lower electronegativity of N versus O [29]. Therefore, the excitation band with the peak at about 272 nm (i.e. 4.57 eV (<5 eV)) can be assigned to the charge transfer (CT) of an electron from N^{3-} to Sm^{3+}, similar to the result of $N^{3-} \rightarrow Sm^{3+}$ charge transfer band (275 nm or 4.51 eV) in $Sr_3Si_{5.8}Al_{2.2}O_{9.2}N_{5.8}$ [2]. On the other hand, there are no signs for the existence of Sm^{2+} observed from the diffuse reflection spectrum and the excitation spectra, even though the sample was prepared in reducing atmosphere. The absence of Sm^{2+} will be further discussed below in relation to the energy level scheme.

As illustrated in Fig. 4 (b), the $Y_{3.88}Sm_{0.12}Si_2O_7N_2$ phosphor exhibits red emission under 272 and 407 nm excitation. The emission spectra of Sm^{3+} exhibits three distinct emission peaks, corresponding to the 4*f* → 4*f* transitions $^4G_{5/2} \rightarrow {}^6H_{5/2}$ at 543 nm, $^4G_{5/2} \rightarrow {}^6H_{7/2}$ at 603 nm, $^4G_{5/2} \rightarrow {}^6H_{9/2}$ at 643 nm [30], respectively. Among them, the predominant emission is the $^4G_{5/2} \rightarrow {}^6H_{7/2}$ transition, while each transition is split because of splitting of the ^6H_x levels. Again there is no straightforward evidence for the existence of Sm^{2+}, because no transition of Sm^{2+} could be identified in the emission spectrum.

3.5. Photoluminescence of $Y_{3.88}Tb_{0.12}Si_2O_7N_2$

$Y_{3.88}Tb_{0.12}Si_2O_7N_2$ emits bright blue-green light under 262 nm

excitation (Fig. 5a). There are two groups of lines in the wavelength range of 350–650 nm in the emission spectrum of $Y_4Si_2O_7N_2$: Tb^{3+}. One group of relatively strong in the range of 475–650 nm relates to the $^5D_4 \rightarrow {}^7F_J$ (J = 6, 5, 4, 3) transitions of Tb^{3+}, and another emission spectra ranging from 350 to 475 nm are attributed to the $^5D_3 \rightarrow {}^7F_J$ (J = 6, 5, 4, 3) transitions of Tb^{3+}. The green emissions from $^5D_4$ to ^7F_J dominate the emission spectrum, and the main peak locates at 544 nm ($^5D_4 \rightarrow {}^7F_5$). In addition, the peak intensity at 544 nm is the maximum value for all Tb^{3+} concentrations under 262 nm excitation.

The dependence of emission peak intensities at 418 nm ($^5D_3 \rightarrow {}^7F_5$, I_{418nm}) and 544 nm ($^5D_4 \rightarrow {}^7F_5$, I_{544nm}) on the Tb^{3+} concentrations upon 262 nm excitation is shown in Fig. 5b. In $Y_{4(1-x)}Tb_{4x}Si_2O_7N_2$, when $x = 0.005$, the value of $I_{418\ nm}$ is similar to that of $I_{544\ nm}$. $I_{418\ nm}$ decreases rapidly with increasing Tb^{3+} concentrations, and the intensities are close to zero above $x = 0.05$ due to cross-relaxation between Tb^{3+} ions [15]. $I_{544\ nm}$ enhances greatly with increasing Tb^{3+} concentrations from $x = 0.01$ to 0.9. When x is at a high value of 0.15, the concentration quenching of $^5D_4$ emission has occurred. The value of r ($^5D_4/^5D_3$) increases greatly with the increasing Tb^{3+} concentrations under the 262 nm excitation, which may be attributed to the cross-relaxation energy transfers processes between neighbouring Tb^{3+} ions through the transitions $^5D_3 \rightarrow {}^5D_4$ and $^7F_6 \rightarrow {}^7F_0$.

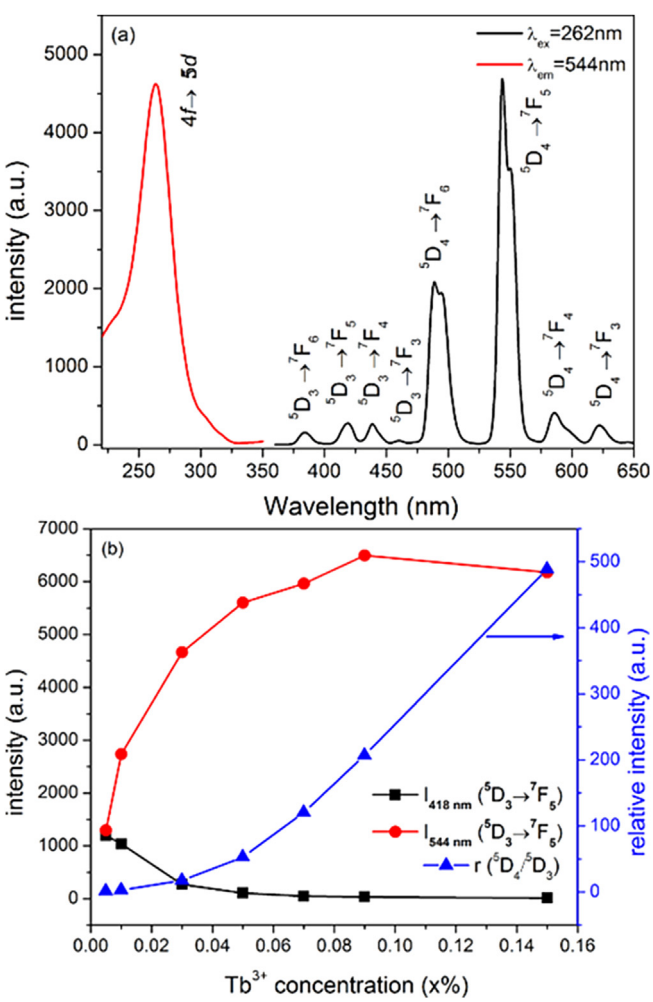

Fig. 5. (a) The excitation and emission spectra of $Y_{3.88}Tb_{0.12}Si_2O_7N_2$. (b) I_{418nm}, I_{544nm} and r($^5D_4/^5D_3$) variation with the increased Tb^{3+} concentration.

The excitation spectrum of $Y_{3.88}Tb_{0.12}Si_2O_7N_2$ is illustrated in Fig. 5(a). The strong broad excitation band with the peak centre at 266 nm (4.67 eV) is attributed to the $4f \rightarrow 5d$ ($4f^8 \rightarrow 4f^7 5d^1$) spin-allowed transition of Tb^{3+} in the host lattice. As is well-known, the ground state of the Tb^{3+} ion with a $4f^8$ electron configuration is the $^7F_6$ level, and its $4f^7 5d^1$ excitation levels contain high-spin (HS) ^9D_J and the low-spin (LS) ^7D_J states. Thus, there are two groups of *f*-*d* transitions in the excitation spectrum of the Tb^{3+} ion, one is the spin-allowed *f*-*d* transition, which is strong and at higher energy region; while another is the spin-forbidden *f*-*d* transition, which is relatively weak and at lower energy region. For Tb^{3+}-doped in $Y_4Si_2O_7N_2$, obviously, the band at 266 nm (4.67 eV) at higher energy region is attributed to spin-allowed $4f \rightarrow 5d$ transition. However, the spin-forbidden $4f \rightarrow 5d$ transition of Tb^{3+} at longer wavelength, which should be located at the position that is 0.75 eV lower in energy than the spin-allowed $4f \rightarrow 5d$ transition of Tb^{3+} [24], has not been observed obviously in the excitation spectrum, due to its extremely weak intensity.

The spin-allowed 4*f*-5*d* transition for the free Tb^{3+} ion is reported to be 62500 cm^{-1} [25]. Thus, the 4*f*-5*d* transition energy E(Tb^{3+}, $Y_4Si_2O_7N_2$) of Tb^{3+} in $Y_4Si_2O_7N_2$ can be calculated to be about 38475 cm^{-1} (260 nm) according to Eq. (2), in good agreement with the experimental result at higher energy region (266 nm).

3.6. Photoluminescence of $Y_{3.88}Er_{0.12}Si_2O_7N_2$

The diffuse reflection and excitation spectra of Er^{3+}-doped $Y_4Si_2O_7N_2$ are illustrated in Fig. 6(a). The optical absorption edge in the wavelength range of 230–290 nm in the reflection spectra is ascribed to the absorption of the host lattice, since there is no obvious difference between un-doped and Er^{3+}-doped sample in higher energy region. In the excitation spectrum, correspondingly, there is a weak excitation band at about 258 nm, which is assigned to the host lattice absorption. In addition, several weak absorption peaks at lower energy were observed in the wavelength range of 350–530 nm, which are attributed to the $4f \rightarrow 4f$ transitions from $^4I_{15/2} \rightarrow {}^2P_{9/2}$(~365 nm), $^4I_{15/2} \rightarrow {}^2P_{11/2}$ (~376 nm), $^4I_{15/2} \rightarrow {}^4G_{9/2}$ (~406 nm), $^4I_{15/2} \rightarrow {}^4F_{5/2}$ (~452 nm), $^4I_{15/2} \rightarrow {}^4F_{7/2}$ (~489 nm) and $^4I_{15/2} \rightarrow {}^4H_{11/2}$ (~522 nm) of Er^{3+} ions, respectively. The most intense excitation peak is at about 376 nm, originating from the $^4I_{15/}$

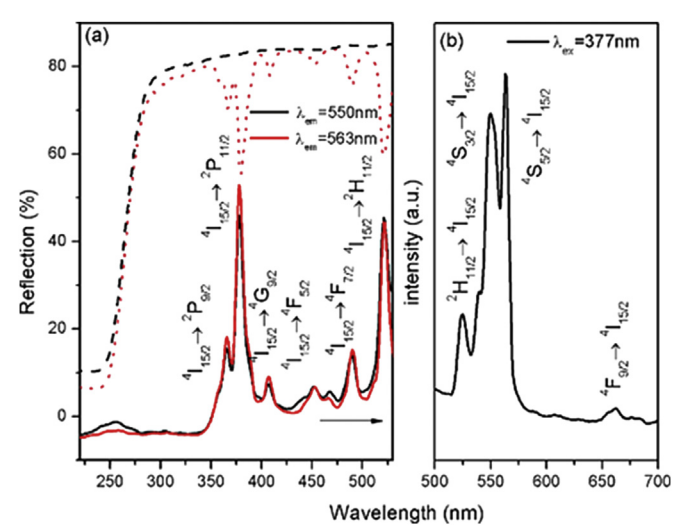

Fig. 6. (a) Diffuse reflection spectrum of Er^{3+}-doped $Y_4Si_2O_7N_2$ (dotted line) compared with un-doped $Y_4Si_2O_7N_2$ (dashed line), and excitation spectra of $Y_{3.88}Er_{0.12}Si_2O_7N_2$. (b) The emission spectra of $Y_{3.88}Er_{0.12}Si_2O_7N_2$.

$_2 \rightarrow {}^2P_{11/2}$ transition. The excitation spectra which consist of a group of peaks from Er^{3+} intra-4*f* transitions are corresponding to the absorption bands observed in the diffuse reflection spectra. Besides, the charge transfer band of the oxygen 2*p* (or nitrogen 3*p*) orbital to the empty 4*f* orbital of Er^{3+} was not definitely detected in the excitation spectra. It was reported that the CT band energy level of Er^{3+} in most of the hosts appeals to be about 0.93 eV higher in energy than that of Sm^{3+} [31]. As aforementioned, the N^{3-}-Sm^{3+} CT energy was 4.57 eV in $Y_4Si_2O_7N_2$:Sm^{3+}. Thus, the N^{3-}-Er^{3+} CT energy should be at 5.5 eV (225 nm), which was not observed in the excitation spectra (Fig. 6a).

As illustrated in Fig. 6 (b), $Y_{3.88}Er_{0.12}Si_2O_7N_2$ exhibits a green emission under 377 nm excitation. Intense emissions at about 550 and 563 nm were observed, due to the transition from ${}^4S_{3/2}$ and ${}^4S_{5/2}$ excited states, respectively, to the ${}^4I_{15/2}$ ground state. Also a weak red emission at about 660 nm was observed, which is assigned to ${}^4F_{9/2} \rightarrow {}^4I_{15/2}$ transition of Er^{3+}.

3.7. Photoluminescence of $Y_{3.88}Dy_{0.12}Si_2O_7N_2$

Fig. 7 (a) shows the diffuse reflection and excitation spectra of $Y_{3.88}Dy_{0.12}Si_2O_7N_2$. The optical absorption edge in the wavelength range of 240–290 nm in the reflection spectra is related to the host lattice absorption as aforementioned. In addition, weak absorption peaks at longer wavelength range of 275–420 nm were observed in the diffuse reflection spectra, which are attributed to the ${}^8S_{7/2} \rightarrow {}^6I_J$ (~294 nm), ${}^8S_{7/2} \rightarrow {}^6P_J$ (~322 nm), ${}^6H_{15/2} \rightarrow {}^8P_{7/2}$ (~350 nm), ${}^6H_{15/2} \rightarrow {}^4I_{11/2}$ (~364 nm), ${}^6H_{15/2} \rightarrow {}^4F_{7/2}$ (~384 nm) and ${}^6H_{15/2} \rightarrow {}^4G_{11/2}$ (~421 nm) transitions of Dy^{3+} ions, respectively. In the excitation spectra, a board band located at about 245 nm (5.07 eV) is observed, which probably can be attributed to the host lattice absorption. It was reported that the CT band energy of Dy^{3+} in most hosts appeals to be about 1.21 eV higher in energy than that of Sm^{3+} [31]. As discussed before, the N^{3-}-Sm^{3+} CT energy was 4.57 eV in $Y_4Si_2O_7N_2$:Sm^{3+}. Thus, the N^{3-}-Dy^{3+} CT energy should be at 5.78 eV (215 nm), which is much larger than the energy of excitation band (5.07 eV) as observed in the excitation spectra. Thus, the excitation band at 245 nm cannot be attributed to the charge transfer band of Dy^{3+}. In addition, this broad excitation band cannot be attributed to 4*f*-5*d* transition of Dy^{3+}, due to the result that the energy of 4*f*-5*d* transition for Dy^{3+} is calculated to be about 50415 cm^{-1} (198 nm)

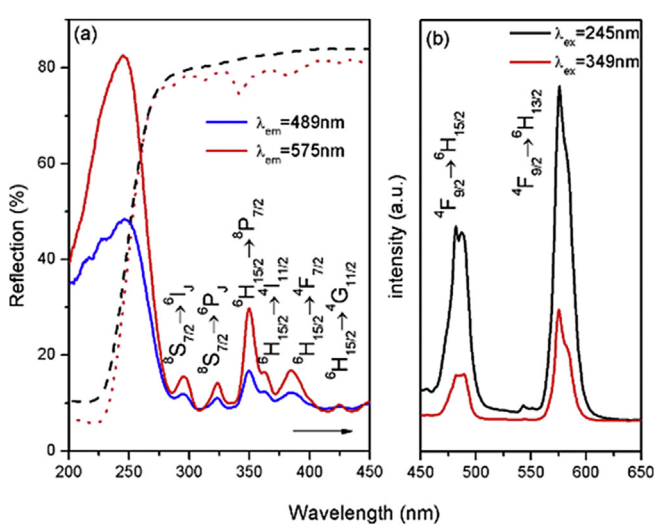

Fig. 7. (a) Diffuse reflection spectrum of Dy^{3+}-doped $Y_4Si_2O_7N_2$ (dotted line) compared with un-doped $Y_4Si_2O_7N_2$ (dashed line), and excitation spectra of $Y_{3.88}Dy_{0.12}Si_2O_7N_2$. (b) Typical emission spectra of $Y_{3.88}Dy_{0.12}Si_2O_7N_2$.

using a $D(Ce^{3+}, Y_4Si_2O_7N_2)$ value of 24025 cm^{-1} and the 4*f*-5*d* transition energy (74440 cm^{-1}) of free Dy^{3+} ion by virtue of Eq. (2) [25]. The excitation peaks in the wavelength range of 275–420 nm attributing to the *f*-*f* transitions of Dy^{3+} were observed, as discussed in the diffuse reflection spectrum.

Fig. 7 (b) illustrates the typical $4f^9 \rightarrow 4f^9$ emission spectra of $Y_{3.88}Dy_{0.12}Si_2O_7N_2$ under 245 and 349 nm excitation. Weak blue-green emission at about 489 and 575 nm were observed and correlated to the transitions from the ${}^4F_{9/2}$ state, to the ${}^6H_{15/2}$ and ${}^6H_{13/2}$ states, respectively.

4. Construction and discussion of the energy level diagram of lanthanides in $Y_4Si_2O_7N_2$

Empirically, the luminescence properties of all trivalent and divalent lanthanides in a specific host can be related to each other by using the energy level scheme, which has originally been developed by P. Dorenbos, the spectroscopic properties of one specific lanthanide, such as Eu^{2+} or Ce^{3+}, in a certain compound can be applied to predict the properties of all other lanthanide ions in the same compound [31–34].

In the energy level scheme, the top of the valence band is usually defined at 0 eV for the convenience of construction and discussion. Accordingly, the energy level scheme for $Y_4Si_2O_7N_2$ can be established by virtue of spectroscopic properties obtained in this work or from the references. The energy level scheme can be constructed using the following steps: (i) The band gap of $Y_4Si_2O_7N_2$ (arrow 1) is estimated to be 5.1 eV (this work). The band gap is defined as the energy of charge transfer from the top of the valence band to the bottom of the conduction band. The value of the band gap is the same as the energy of the host lattice excitation band at 4.7 eV plus an estimated 0.4 eV for the electron-hole binding energy in the exciton [35]. (ii) In order to determine the 4*f* ground state of Ln^{2+}, the information on the CT band of Ln^{3+} can be used to indicate the energy difference between the 4*f* ground state of Ln^{2+} and the top of the valence band. The energy of the Sm^{3+} CT band about 4.57 eV (this work) equals the energy difference between the 4*f* ground state of Sm^{2+} and the top of the valence band (arrow 2). (iii) The wavelength of the first $4f^7$-$4f^65d$ transition in Eu^{2+} is estimated near 420 nm from the Eu^{2+} excitation spectra from G. Z. Chen et al. [22] The corresponding energy of 2.96 eV (arrow 3) then provides the energy difference between the lowest 4*f* and lowest 5*d* states of all other divalent ions. (iv) To position the energy levels of the trivalent ions with respect to the valence and conduction band, one needs either the CT band of any Ln^{4+} ion which relates the lowest 4*f* state of the Ln^{3+} ion level to the top of the valence band, or the thermal quenching data on the 5*d*-4*f* emissions of the Ln^{3+} ion which relate the 5*d* levels to the bottom of the conduction band. However, no information on Ln^{4+} ions in $Y_4Si_2O_7N_2$ is available. Fortunately, the thermal quenching data of 5*d*-4*f* emissions of the Ce^{3+} ion in $Y_4Si_2O_7N_2$ has been reported [19], and the position of the lowest Ce^{3+} 5*d* energy level is roughly estimated to be 0.28 eV below the bottom of the conduction band, as shown in the blue arrow in Fig. S2 (supporting information). (v) The position of the lowest 4*f* energy level of Ln^{3+} in $Y_4Si_2O_7N_2$ can be derived from the excitation spectra of the Ce^{3+} *d*-*f* emission band. The 4*f*-5*d* absorption band of Ce^{3+} (3.03 eV, arrow 4) obtained by J.W.H. van Krevel [14] and Q. Wu et al. [19], was used to determine the energy difference between the lowest 4*f* ground state and lowest 5*d* excited state of the trivalent lanthanide ions in $Y_4Si_2O_7N_2$.

The energy level scheme is a powerful tool for the interpretation and prediction of the excitation, emission and absorption of lanthanides in a certain host lattice. For Pr^{3+}-doped sample, by comparing Fig. 8 with Fig. 3 (a), the $4f^2 \rightarrow 4f^15d^1$ transition of Pr^{3+} in $Y_4Si_2O_7N_2$ predicted from energy level scheme is 4.51 eV, which

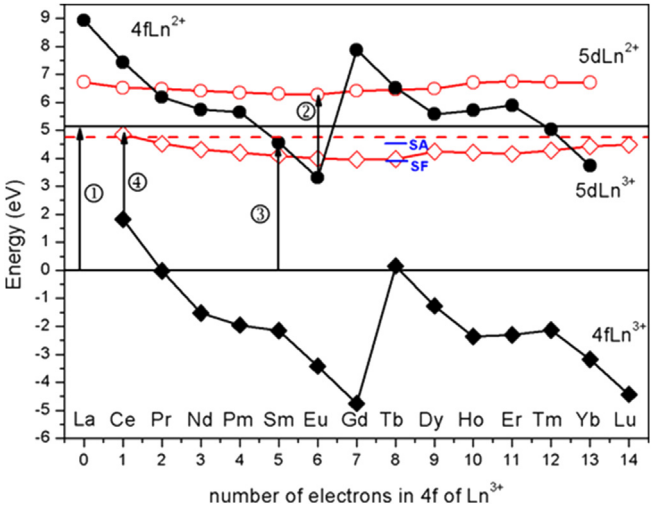

Fig. 8. Energy level scheme showing the 4*f* ground states of the trivalent (filled square) and divalent ions (filled circle) and lowest energy 5*d* states of the trivalent (open square) and divalent ions (open circle) relative to the valence and conduction band of $Y_4Si_2O_7N_2$. The red dashed horizontal line is the optical band gap of $Y_4Si_2O_7N_2$. The arrows (1–4) indicate the experimentally determined transitions used to construct this scheme. (For interpretation of the references to colour in this figure legend, the reader is referred to the web version of this article.)

is in good agreement with the 4*f*-5*d* transition (4.51 eV) of Pr^{3+} observed in this work (Section 3.3). Similarly, the spin-forbidden (SF) and spin-allowed (SA) 4*f*-5*d* transitions of Tb^{3+} predicted from energy level scheme are 3.78 and 4.53 eV, respectively, which is little lower in energy than that the spin-allowed 4*f*-5*d* transition (4.67 eV) of Tb^{3+} observed in this work (Section 3.5). And the error might be attributed to the overlap of the host lattice absorption at 245 nm and the excitation band of Pr^{3+} was at 275 nm.

Furthermore, the energy level scheme can be used to discuss the preferred divalent and trivalent states of lanthanide ions in $Y_4Si_2O_7N_2$. When the energy difference between the ground state of Ln^{2+} ion and the bottom of the conduction band is large, the Ln^{2+} ion will be more stable and it would be more likely that a divalent ion is formed during the preparation process, such as Eu^{2+} in $CaAlSiN_3$ [33]. On the other hand, if it is the other way around it, the 4*f* ground state of the divalent ion is near to the conduction band, the lanthanide ion gives up an electron to the conduction band easily and would be more stable in the trivalent state, such as Ce^{3+}, Pr^{3+} and Sm^{3+}. Take Sm for an example, due to the fact that the 4*f* ground state of Sm^{2+} is about 1.21 eV higher in energy than that of Eu^{2+}, the 4*f* ground state of Sm^{2+} is more near to the conduction band other than to the valence band. Thus, Sm is expected to exist in the trivalent state in $Y_4Si_2O_7N_2$ which is in agreement with the observation from our research. Despite the sample was sintered in a reducing atmosphere (N_2/H_2 = 95: 5), Sm^{3+} has not been converted into Sm^{2+}. For the same reason, Tm and Yb should exist in the trivalent state in the $Y_4Si_2O_7N_2$, since the fact that the 4*f* states of Tm^{2+} and Yb^{2+} are 1.72 and 0.5 eV higher in energy than that of Eu^{2+}, respectively.

The energy level scheme can be used to predict the luminescence properties of other (not yet studied) lanthanide ions in the specific host lattice. Tm and Yb, similar to Sm, acted as trivalent ions when they were introduced into the host lattice, have a CT band and give typical 4*f*-4*f* emission in the visible region. Other rare-earth ions (e.g. Ce, Pr and Tb) will be in the trivalent state or have a CT energy higher than the band gap of $Y_4Si_2O_7N_2$. So, it can be concluded from the energy level scheme that Sm^{3+}, Tm^{3+} and Yb^{3+} may act as shallow electron traps in $Y_4Si_2O_7N_2$ as their divalent ground states are actually below the conduction band. However, Ce^{3+} is the only rare-earth ion that can act as a stable hole trap, due to the fact that its ground state is above the valence band.

5. Conclusion

$Y_{3.88}RE_{0.12}Si_2O_7N_2$ (RE = Pr, Sm, Tb, Er, Dy) samples were prepared by a solid-state reaction at high temperature, and their photoluminescence properties were investigated. The host absorption is located at about 250 nm. The direct Pr^{3+} $4f^2 \rightarrow 4f^15d^1$ excitation at 275 nm leads to typical $4f^2 \rightarrow 4f^2$ emission peaks (450–700 nm) and strong $4f^15d^1 \rightarrow 4f^2$ emission band (300–450 nm). The charge transfer band of Sm^{3+} located at about 272 nm is rather low due to a lower electronegativity of N compared with O, and typical red emissions ($4f^2 \rightarrow 4f^2$) of Sm^{3+} were observed under 272 nm excitation. In addition, the spin-allowed $f \rightarrow d$ transition of Tb^{3+} in $Y_4Si_2O_7N_2$ is observed at 266 nm, the 4*f*-4*f* Tb^{3+} emission lines mainly from the $^5D_4$ level were also observed. The incorporation of Er^{3+} (or Dy^{3+}) into $Y_4Si_2O_7N_2$ resulted in a typical Er^{3+} (or Dy^{3+}) *f*-*f* line absorptions and emissions. The energy level diagram showing the position of 4*f* and 5*d* energy levels of all divalent and trivalent lanthanide ions relative to the valence and conduction band of $Y_4Si_2O_7N_2$ has been established and studied.

Acknowledgements

This work was supported by the National Natural Science Foundation of China under Grant No. 11104298, 51171239, U1332202, Shanghai University Innovation Program and Shanghai School Young Teacher Program. The authors thank Dr. Ang Feng (Ghent University) for the calculation of binding energy using first principle method.

Appendix A. Supplementary data

Supplementary data related to this article can be found at http://dx.doi.org/10.1016/j.jallcom.2017.02.298.

References

[1] C.N. Zhang, T. Uchikoshi, R.J. Xie, L.H. Liu, Y.J. Cho, Y. Sakka, N. Hirosaki, T. Sekiguchi, Reduced thermal degradation of the red-emitting $Sr_2Si_5N_8$:Eu^{2+} phosphor via thermal treatment in nitrogen, J. Mater. Chem. C. 3 (2015) 7642–7651.
[2] X.J. Wang, L. Wang, T. Takeda, S. Funahashi, T. Suehiro, N. Hirosaki, R.J. Xie, Blue-emitting $Sr_3Si_{8-x}Al_xO_{7+x}N_{8-x}$:$Eu^{2+}$ discovered by a single-particle-diagnosis approach: crystal structure, luminescence, scale-up synthesis, and its abnormal thermal quenching behavior, Chem. Mater. 27 (2015) 7689–7697.
[3] Y.T. Tsai, C.Y. Chiang, W.Z. Zhou, J.F. Lee, H.S. Sheu, R.S. Liu, Structural ordering and charge variation induced by cation substitution in (Sr,Ca)$AlSiN_3$:Eu phosphor, J. Am. Chem. Soc. 137 (2015) 8936–8939.
[4] W.B. Park, S.P. Singh, K.S. Sohn, Discovery of a phosphor for light emitting diode applications and its structural determination, $Ba(Si,Al)_5(O,N)_8$:Eu^{2+}, J. Am. Chem. Soc. 136 (2014) 2363–2373.
[5] X.C. Wang, Z.Y. Zhao, Q.S. Wu, Y.Y. Li, C. Wang, A.J. Mao, Y.H. Wang, Synthesis, structure, and luminescence properties of $SrSiAl_2O_3N_2$:Eu^{2+} phosphors for light-emitting devices and field emission displays, Dalton Trans. 44 (2015) 11057–11066.
[6] S. Schmiechen, P. Strobel, C. Hecht, T. Reith, M. Siegert, P.J. Schmidt, P. Huppertz, D. Wiechert, W. Schnick, Nitridomagnesosilicate $Ba[Mg_3SiN_4]$:Eu^{2+} and structure–property relations of similar narrow-band red nitride phosphors, Chem. Mater. 27 (2015) 1780–1785.
[7] W.B. Park, S.P. Singh, M. Kim, K.S. Sohn, Combinatorial screening of luminescent and structural properties in a Ce^{3+}-doped Ln-Al-Si-O-N (Ln = Y, La, Gd, Lu) system: the discovery of a novel $Gd_3Al_{3+x}Si_{3-x}O_{12+x}N_{2-x}$:$Ce^{3+}$ phosphor, Inorg. Chem. 54 (2015) 1829–1840.
[8] V. Bachmann, C. Ronda, O. Oeckler, W. Schnick, A. Meijerink, Color point tuning for (Sr,Ca,Ba)$Si_2O_2N_2$:Eu^{2+} for white light LEDs, Chem. Mater. 21 (2009) 316–325.

[9] L. Wang, X.G. Wang, T. Takeda, N. Hirosaki, Y.T. Tsai, R.S. Liu, R.J. Xie, Structure, luminescence, and application of a robust carbidonitride blue phosphor $Al_{1-x}Si_xC_xN_{1-x}$:Eu^{2+} for near UV-LED driven solid state lighting, Chem. Mater. 27 (2015) 8457–8466.
[10] G.G. Li, Y. Tian, Y. Zhao, J. Lin, Recent progress in luminescence tuning of Ce^{3+} and Eu^{2+}-activated phosphors for pc-WLEDs, Chem. Soc. Rev. 44 (2015) 8688–8713.
[11] F.C. Lu, X.P. Song, Q.L. Liu, Crystal structure and photoluminescence properties of $(Y_{1-x}Ce_x)_4Si_2O_7N_2$, Opt. Mater. 33 (2010) 91–98.
[12] X. Xu, C. Cai, L.Y. Hao, Y.C. Wang, Q.X. Li, The photoluminescence of Ce-doped $Lu_4Si_2O_7N_2$ green phosphors,, Mater. Chem. Phys. 118 (2009) 270–272.
[13] J. Takahashi, H. Yamane, N. Hirosak, Y. Yamamoto, T. Suehiro, T. Kamiyama, M. Shimada, Crystal structure of $La_4Si_2O_7N_2$ analyzed by the rietveld method using the time-of-flight neutron powder diffraction data, Chem. Mater. 15 (2003) 1099–1104.
[14] J.W.H. van Krevela, H.T. Hintzen, R. Metselaar, A. Meijerink, Long wavelength Ce^{3+} emission in Y-Si-O-N materials, J. Alloys Compd. 268 (1998) 272–277.
[15] F.C. Lu, L.J. Bai, Y. Lu, W. Dang, Z.P. Yang, P. Lin, Photoluminescence mechanism and thermal stability of Tb^{3+}-Doped $Y_4Si_2O_7N_2$ green-emitting phosphors, J. Am. Ceram. Soc. 98 (2015) 867–872.
[16] J. Yang, J. Feng, M. Zhao, X.R. Ren, W. Pan, Electronic structure, mechanical properties and anisotropy of thermal conductivity of Y-Si-O-N quaternary crystals, Comput. Mater. Sci. 109 (2015) 231–239.
[17] K.J.D. MacKenzie, G.J. Gainsford, M.J. Ryan, Rietveld refinement of the crystal structures of the yttrium silicon oxynitrides $Y_2Si_3N_4O_3$ (N-Melilite) and $Y_4Si_2O_7N_2$ (J-Phase), J. Eur. Ceram. Soc. 16 (1996) 553–560.
[18] Y.H. Song, N. Guo, H.P. You, Synthesis and luminescent properties of cerium-, terbium-, or dysprosium-doped $Gd_4Si_2O_7N_2$ materials, Eur. J. Inorg. Chem. 14 (2011) 2327–2332.
[19] Q.S. Wu, Z.G. Yang, Z.G. Zhao, M.D. Que, X.C. Wang, Y.H. Wang, Synthesis, crystal structure and luminescence properties of a $Y_4Si_2O_7N_2$:Ce^{3+} phosphor for near-UV white LEDs, J. Mater. Chem. C. 2 (2014) 4967–4973.
[20] Z.G. Xia, W.W. Wu, Preparation and luminescence properties of Ce^{3+} and Ce^{3+}/Tb^{3+}-activated $Y_4Si_2O_7N_2$ phosphors, Dalton Trans. 42 (2013) 12989–12997.
[21] C.M. Fang, G.A. de Wijs, R.A. de Groot, R. Metselaar, H.T. Hintzen, G. de With, O/N ordering in $Y_2Si_3O_3N_4$ with the melilite-type structure from first-principles calculations, Chem. Mater. 12 (2000) 1071–1075.
[22] G.Z. Chen, L.J. Yin, J.T. Dong, Y.Y. Feng, Y. Gao, W.D. He, Y. Jia, X. Xu, H.T. Hintzen, Synthesis, crystal structure, and luminescence properties of $Y_4Si_2O_7N_2$: Eu^{2+} oxynitride phosphors, J. Am. Ceram. Soc. 99 (2016) 183–190.
[23] R.D. Shannon, Revised Effective ionic radii and systematic studies of interatomie distances in halides and chaleogenides, Acta Cryst. 32 (1976) 17.
[24] Z.J. Zhang, O.M. ten Kate, A. Delsing, P. Dorenbos, J.T. Zhao, H.T. Hintzen, Photoluminescence properties of Pr^{3+}, $Sm^{3+}$and Tb^{3+} doped $SrAlSi_4N_7$ and energy level locations of rare-earth ions in $SrAlSi_4N_7$, J. Mater. Chem. C. 2 (2014) 8.
[25] P. Dorenbos, Predictability of 5d level positions of the triply ionized lanthanides in halogenides and chalcogenides, J. Lumin. 87 (2000) 970–972.
[26] P. Dorenbos, The 5d level positions of the trivalent lanthanides in inorganic compounds, J. Lumin. 91 (2000) 155–176.
[27] N.J.M. Le Masson, A.P. Vink, P. Dorenbos, A.J.J. Bos, C.W.E. VanEijk, J.P. Chaminade, Ce^{3+} and Pr^{3+} 5d-energy levels in the (pseudo) perovskites $KMgF_3$ and $NaMgF_3$, J. Lumin. 101 (2003).
[28] L.L. Wang, H.M. Noh, B.K. Moon, S.H. Park, K.H. Kim, J. Shi, J.H. Jeong, Dual-mode luminescence with broad near UV and blue excitation band from Sr_2CaMoO_6:Sm^{3+} phosphor for white LEDs, J. Phys. Chem. C. 119 (2015) 15517–15525.
[29] W.B. Park, S.P. Singh, M. Pyo, K.S. Sohn, $Y_{6+x/3}Si_{11-y}Al_yN_{20+x-y}O_{1-x+y}$:$Re^{3+}$ (Re = Ce^{3+}, Tb^{3+}, Sm^{3+}) phosphors identified by solid-state combinatorial chemistry, J. Mater. Chem. 21 (2011) 5780.
[30] A. Watras, P.J. Deren, R. Pązik, Luminescence properties and determination of optimal RE^{3+}(Sm^{3+}, $Tb^{3+}$and Dy^{3+}) doping levels in the KYP_2O_7 host lattice obtained by combustion synthesis, New J. Chem. 38 (2014) 5058–5068.
[31] P. Dorenbos, Lanthanide charge transfer energies and related luminescence, charge carrier trapping, and redox phenomena, J. Alloys Compd. 488 (2009) 568–573.
[32] P. Dorenbos, Absolute location of lanthanide energy levels and the performance of phosphors, J. Lumin. 122 (2007) 315–317.
[33] Z.J. Zhang, O.M. ten Kate, A. Delsing, E. van der Kolk, P.H.L. Notten, P. Dorenbos, J.T. Zhao, H.T. Hintzen, Photoluminescence properties and energy level locations of RE^{3+} (RE = Pr, Sm, Tb, Tb/Ce) in $CaAlSiN_3$ phosphors, J. Mater. Chem. 22 (2012) 9813–9820.
[34] L.X. Ning, C.C. Zhou, W.P. Chen, Y.C. Huang, C.K. Duan, P. Dorenbos, Y. Tao, H.B. Liang, Electronic properties of Ce^{3+}-Doped $Sr_3Al_2O_5Cl_2$: a combined spectroscopic and theoretical study, J. Phys. Chem. C. 119 (2015) 6785–6792.
[35] O.M. ten Kate, Z. Zhang, P. Dorenbos, H.T. Hintzen, E. van der Kolk, 4f and 5d energy levels of the divalent and trivalent lanthanide ions in $M_2Si_5N_8$ (M=Ca, Sr, Ba), J. Solid State Chem. 197 (2013) 209–217.